Role of Substrate in Directing the Self-Assembly of Multicomponent Supramolecular Networks at the Liquid–Solid Interface

Tatyana Balandina,[†] Kazukuni Tahara,[‡] Nadja Sändig,[§] Matthew O. Blunt,[†] Jinne Adisoejoso,[†] Shengbin Lei,[⊥] Francesco Zerbetto,[§,*] Yoshito Tobe,[‡,*] and Steven De Feyter[†,*]

[†]Department of Chemistry, Division of Molecular Imaging and Photonics, KU Leuven, Celestijnenlaan 200 F, B-3001, Leuven, Belgium, [‡]Division of Frontier Materials Science, Graduate School of Engineering Science, Osaka University Toyonaka, Osaka 560-8531, Japan, [§]Dipartimento di Chimica "G. Ciamician", Università di Bologna, V. F. Selmi 2, 40126 Bologna, Italy, and [⊥]Key Laboratory of Microsystems and Microstructures Manufacturing, Ministry of Education, Harbin Institute of Technology, Harbin, 150080, People's Republic of China.

ABSTRACT The self-assembly of multicomponent networks at the liquid–solid interface between Au(111) or highly oriented pyrolytic graphite (HOPG) and organic solvents was investigated using scanning tunneling microscopy. Alkoxylated dehydrobenzo[12]annulene (DBA) derivatives form hexagonal nanoporous networks, which trap either single molecules of coronene (COR) or small clusters of COR and isophthalic acid to form multicomponent networks. The pattern of interdigitation between alkyl chains from DBA molecules produces hexagonal pores that are either chiral or achiral. On Au(111) substrates multicomponent networks display an ordered superlattice arrangement of chiral and achiral pores. In comparison, similar networks on HOPG display only chiral pores. The unique superlattice structure observed on Au(111) is related to a lower energetic preference for chiral pores than on HOPG and increased diffusion barriers for guest molecules. The increased diffusion barriers for guests allow them to act as nucleation sites for the formation of achiral pores. Following the initial nucleation of an achiral pore, restrictions imposed by the accommodation of guests within the porous network mean that subsequent growth naturally leads to the formation of the superlattice structure.

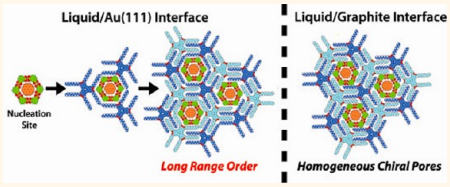

KEYWORDS: host–guest systems · Au(111) · scanning tunnelling microscopy · self-assembly · substrate effect · solid–liquid interface

Control over the self-assembly of molecular building blocks into well-defined architectures at surfaces represents one of the most important challenges of contemporary supramolecular chemistry. Two-dimensional (2D) crystalline monolayers based on physisorbed molecules display the potential for applications such as selective guest adsorption,[1,2] chiral recognition,[3,4] and the formation of 2D polymers.[5,6] In addition these structures also provide a testing ground in which to study the physical processes associated with molecular self-assembly.

Surface-confined 2D molecular crystals have been widely studied using scanning tunneling microscopy (STM) at the liquid–solid interface[2,7−11] and under UHV.[12−14] In particular, 2D porous networks constructed of initially nonporous building blocks have attracted a large amount of interest. These porous networks are typically sustained *via* hydrogen bonds,[9,15−17] metal–ligand coordination,[13,14,18] or even van der Waals interactions.[19,20] The advantage of these porous networks is that the size and geometry of the pores can be easily changed by adjusting the size and symmetry of the building blocks. An important application for such 2D nanoporous networks is the trapping of functional guest molecules in a repetitive and spatially ordered arrangement on a surface.[21,22]

Self-assembly from solution is a complex process that relies on a balance of intermolecular (molecule–molecule and molecule–solvent) and interfacial (molecule–substrate and solvent–substrate) interactions. Recent studies have shown the importance of solvent,[7,9,23,24] solute concentration,[25,26] temperature,[27,28] and substrate.[29−31] The complexity of the self-assembly process is magnified for networks consisting of more than one type of building block. One of the main obstacles for multicomponent networks is phase separation of the individual components.[30,32] This has meant the occurrence of multicomponent networks, especially those with three or more components, is rare.[33−35] Recently, we were able to demonstrate the formation of three-[36] and

* Address correspondence to francesco.zerbetto@unibo.it, tobe@chem.es.osaka-u.ac.jp, steven.defeyter@chem.kuleuven.be.

Received for review July 13, 2012 and accepted August 26, 2012.

Published online September 06, 2012
10.1021/nn303144r

four[22]-component networks on an HOPG substrate based on alkylated dehydrobenzo[12]annulene (DBA) derivatives with combinations of isophthalic acid (ISA), coronene (COR), and triphenylene.

Here we demonstrate for the first time the use of different substrate materials, HOPG and Au(111), for the formation of multicomponent networks with identical composition but different long-range order. The different surfaces affect the strength of molecule–substrate interactions and the mobility of adsorbed species and subsequently their ability to act as nucleation sites for growth of the network. These effects combine to produce a subtly different structural ordering of the networks on the different substrates, highlighting the important role that the substrate plays in determining the growth of 2D molecular multicomponent networks.

RESULTS AND DISCUSSION

Molecular Building Blocks. DBA derivatives form nanoporous networks with hexagonal symmetry stabilized by van der Waals interactions between interdigitated pairs of alkyl chains.[26,37] The edge of each hexagonal nanowell consists of a pair of alkyl chains from one DBA molecule, interdigitated with a pair from an adjacent molecule. When adsorbed on a surface, this interdigitation becomes chiral with two distinct interdigitation motifs, labeled arbitrarily (−) and (+) (Figure 1A, see corresponding shift of DBA cores with respect to each other). The combination of interdigitation motifs within an individual nanowell can produce either chiral or achiral nanowells. Chiral nanowells have a combination of six identical interdigitation motifs, either all (−) or all (+) (Figure 1B, nanowell with (+) interdigitations is shown) and have 6-fold rotational symmetry. Monocomponent systems of DBA on HOPG have been shown to form networks with domains of nanowells all showing a single chirality.[26] Achiral pores have a combination of three (−) and three (+) interdigitation motifs arranged in an alternating pattern (Figure 1B).

Varying the alkyl chain length of the DBA derivative allows tuning of the pore size to trap specific guest molecules, or collections of guest molecules, to form multicomponent structures.[36,38] The systems presented here consist of combinations of DBAs with either hexyloxy (DBA-OC6) or decyloxy (DBA-OC10) chains, COR, and ISA (see Scheme 1 for molecular structures and SI for the synthesis of DBA-OC6).

Molecular modeling suggests that the size and shape of COR fit the nanowell formed by a hexamer of DBA-OC6, forming a two-component network composed of DBA-OC6 and COR (Figure 1C). In addition, the formation of a three-component network composed of DBA-OC10, COR, and ISA (Figure 1D) has been previously reported on an HOPG surface.[36] Six molecules of ISA self-assemble into a hydrogen-bonded ring around one COR. This COR/ISA heterocomplex has been shown to be a particularly stable supramolecular arrangement and forms a three-component network when adsorbed in the hexagonal DBA-OC10 nanowell.

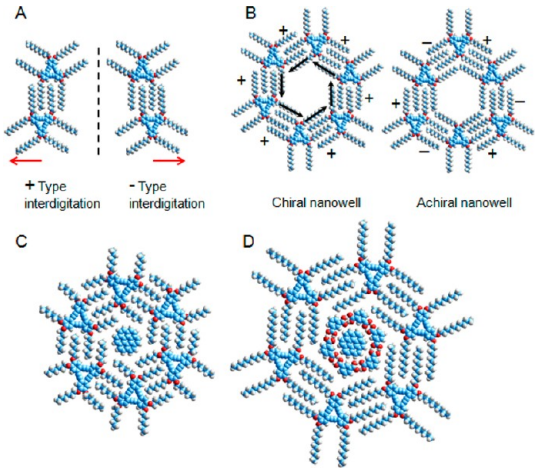

Figure 1. (A) Molecular models of (+) and (−) interdigitation patterns. Red arrows indicate corresponding shift of the bottom DBA core with respect to the upper one. (B) Molecular models of chiral and achiral nanowells. The latter can be formed by different combinations of (+)- and (−)-type interdigitation patterns. The black arrows in (B) indicate the chirality of the pore. Molecular models of the (C) two- and (D) three-component systems.

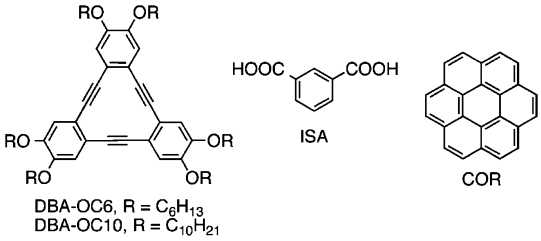

Scheme 1. Chemical structures of DBA-OC6, DBA-OC10, COR, and ISA.

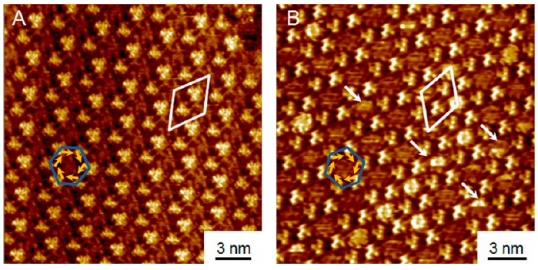

Figure 2. STM images of a monolayer formed from a one-component (DBA-OC6) and two-component (DBA-OC6/COR) solution in TCB on HOPG: (A) $C_{(DBA\text{-}OC6)}$ = 1.3 × 10^{-4} M; conditions: I_{set} = 100 pA, V_{set} = −700 mV. (B) $C_{(DBA\text{-}OC6)}$ = 6.5 × 10^{-5} M, $C_{(COR)}$ = 1.8 × 10^{-3} M; conditions: I_{set} = 80 pA, V_{set} = −735 mV. $C_{(X)}$ reflects the concentration of component X in the supernatant solution, prior to adsorption. The white outlines in (A) and (B) indicate the unit cells of the honeycomb structure. Blue hexagons with yellow arrows along alkyl chains in (A) and (B) indicate chirality of the nanowells (also based on the corresponding shift of DBA cores with respect to each other). White arrows in (B) show nanowells with mobile COR molecules.

One- (DBA-OC6) and Two-Component (DBA-OC6/COR) Networks on HOPG. Previously we reported the formation of the honeycomb structure of DBA derivatives with long alkyl chains (longer than $C_{10}H_{21}$).[26] DBA with six hexyloxy chains similarly forms chiral honeycomb structures at the 1,2,4-trichlorobenzene (TCB)/graphite interface (Figure 2A). Individual domains contain only chiral pores with either all (+) or all (−) interdigitation patterns. Two-component networks formed by DBA-OC6 and COR on HOPG display the same nanowell chirality as monocomponent DBA networks and show identical unit cell parameters 2.6 ± 0.1 nm, $\gamma = 62 \pm 3°$ (Figure 2B). Figure 2B shows a typical STM image of two-component networks consisting of DBA-OC6 and COR in TCB on HOPG. The DBA moieties appear as bright triangular features due to the unsaturated annulene core, and alkoxy chains appear as darker lines between adjacent DBA cores.[3] Both images in Figure 2 show domains where only the (−)-type interdigitation pattern is present, as depicted by blue overlaid hexagons with yellow arrows. COR molecules appear as fuzzy bright disks with a diameter of ∼1 nm trapped within the nanowells (Figure 2B). Note however that only a small fraction of the pores are occupied by COR molecules, leaving the majority vacant (*vide infra*). Some nanowells (indicated by white arrows in Figure 2B) appear partially filled with COR molecules. This effect results from mobile COR molecules that can enter or leave pores between scan lines of the STM image, resulting in pores that appear partially filled. Differences in contrast for trapped COR are in line with previously reported results for a trimesic acid/COR system on HOPG, where contrast modulation was explained by a varying interaction with the substrate, rotation of the COR guests, or a combination thereof.[2]

One- (DBA-OC6, COR) and Two-Component (DBA-OC6/COR, COR/ISA) Networks on Au(111). With careful control of the concentration, monocomponent solutions of DBA-OC6 at the TCB/Au(111) interface also form porous patterns. Interestingly, the majority of pores display a distorted form, consisting of unequal combinations of (+)- and (−)-type interdigitation motifs (Figure 3A, distorted hexagons are overlaid with yellow features). The remaining pores in this monocomponent system are chiral or achiral and have been overlaid with blue and red/green outlines, respectively. Figure 3B demonstrates molecular models for all three types of pore (chiral, achiral, and distorted) that are observed on Au(111). These results are in sharp contrast to the formation of the monocomponent structure on HOPG, which forms domains displaying only chiral pores with a single chirality (Figure 2A).

Deposition of a premixed solution of the two components (DBA-OC6/COR) allowed us to form two-component networks on Au(111) (Figure 3B). Highly ordered domains of self-assembled networks extended over regions more than 50 × 50 nm in size (Figure S1) and covered the fcc-bridge-hcp regions of the herringbone structure of ($\sqrt{3}\times22$) Au(111). Bright humps in Figure 3B running from the lower left to upper right corner reflect ridges of the herringbone reconstructed Au(111). The two-component network on Au(111) is similar to that on HOPG, showing a porous framework formed by DBA with pores containing a single COR. In contrast to HOPG however two-component networks on Au(111) display an ordered pattern of both chiral and achiral nanowells within individual nanoporous domains. The basis of this *superlattice* structure is a chiral nanowell surrounded by six achiral nanowells (Figure 3B, the blue hexagon indicates a chiral nanowell; red and green hexagons indicate achiral nanowells with different orientations). The two-component superlattice network was characterized by the following unit cell: $a = b = 6.0 \pm 0.2$ nm, $\gamma = 52 \pm 2°$, schematically drawn by the white outline in Figure 3B. Unit cell vectors are rotated 7.8 ± 3° clockwise with respect to the ⟨110⟩ direction of Au(111). Interestingly the adsorption of COR is observed clearly only within achiral nanowells. In chiral nanowells COR molecules appear as less well-defined features, and in some cases two CORs are adsorbed, as indicated by the white arrow in the left upper corner of Figure 3B. This is attributed to a more tight packing in the achiral nanowells.

The two-component system composed of DBA-OC6 and COR at the TCB/Au(111) interface shows complete occupancy of nanowells by COR (Figure 3B). This differs from the identical system on HOPG, where STM images show only 25.0 ± 4% of the DBA-OC6 pores are occupied by COR (Figure 2B). This occurs despite there being 10 times as much COR present in solution for HOPG as compared to Au(111). These observations are in line with previously reported smaller desorption energies of benzene from HOPG[39−41] (11.5 kcal mol^{-1}) as compared to Au(111) (13.8 kcal mol^{-1}).[42] Benzene and COR are both aromatic compounds and are expected to follow the same trend.

Smaller desorption energies of benzene-related molecules from HOPG rather than Au(111) effect the formation of monocomponent networks of COR. Under our experimental conditions monocomponent networks of COR were never observed on HOPG with STM (using either TCB or 1-octanoic acid as solvents). In contrast, on Au(111) the formation of a densely packed monolayer with the *p*6 plane group is readily observed for COR in either TCB (Figure S2) or 1-octanoic acid (Figure 4A). The monolayer of COR in 1-octanoic acid was found to be stable, with only a few defects, caused by desorbed COR moieties observed. The unit cell ($a = b = 1.0 \pm 0.1$ nm, $\gamma = 57.0 \pm 1°$) consists of a single COR molecule with unit cell vectors *a* and *b* aligned nearly parallel to the ⟨110⟩ directions of the Au(111) substrate.

Saturated mixtures of COR and ISA in 1-octanoic acid on HOPG give rise predominantly to COR/ISA heterocluster formation.[11] On Au(111) however, such heteroclusters are observed only by carefully controlling the concentration of both components (Figure 4B), with COR as the minority component (COR/ISA ratio is equal to 1/600).

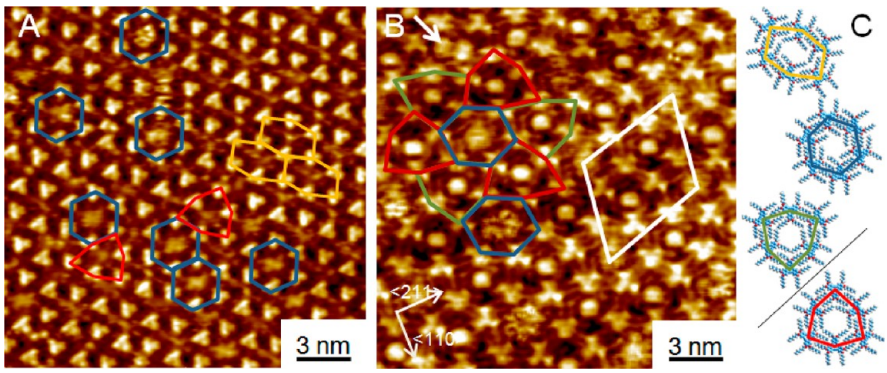

Figure 3. STM images of a monolayer formed from one-component (DBA-OC6) and two-component (DBA-OC6/COR) solutions at the TCB/Au(111) interface: (A) $C_{(DBA\text{-}OC6)} = 1.3 \times 10^{-4}$ M, the majority of hexagons have a distorted shape (examples are overlaid in yellow); conditions: $I_{set} = 100$ pA, $V_{set} = -350$ mV. (B) $C_{(DBA\text{-}OC6)} = 6.5 \times 10^{-5}$ M, $C_{(COR)} = 1.8 \times 10^{-4}$ M; conditions: $I_{set} = 80$ pA, $V_{set} = -380$ mV. The white outline indicates the unit cell of the superlattice structure. The white arrow in the upper left corner shows the presence of two COR molecules within a single chiral nanowell. Directions of gold lattice are shown by white arrows. Blue hexagons in (A) and (B) indicate chiral nanowells; red and green hexagons indicate achiral pores with different orientations. $C_{(X)}$ reflects the concentration of component X in the supernatant solution prior to adsorption. (C) Molecular models for all types of hexagons observed on Au(111).

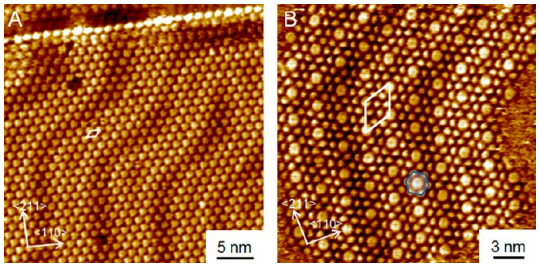

Figure 4. STM images of monolayers formed at the 1-octanoic acid/Au(111) interface from a solution of (A) COR, $C_{(COR)} = 5.0 \times 10^{-4}$ M; conditions: $I_{set} = 100$ pA, $V_{set} = -270$ mV; (B) two-component mixture of COR and ISA, $C_{(ISA)} = 2.5 \times 10^{-3}$ M, $C_{(COR)} = 4.2 \times 10^{-6}$ M; conditions: $I_{set} = 390$ pA, $V_{set} = -465$ mV. One COR/ISA heteromolecular cluster is highlighted in blue. The corners of the hexagon coincide with the isophthalic acid groups. Unit cells are indicated in white; directions of gold lattice are shown by white arrows.

The repeating unit for the COR/ISA monolayer on Au(111) (Figure 4B) consists of one COR and six ISA molecules, with the following unit cell dimensions: $a = b = 2.3 \pm 0.1$ nm and $\gamma = 59 \pm 1°$. These values are perfectly in line with those on graphite ($a = b = 2.3 \pm 0.04$ nm and $\gamma = 59 \pm 1°$).[36] Reconstruction lines of Au(111) were stable, following the ⟨211⟩ directions of Au(111), and were not lifted upon the formation of either COR or COR/ISA monolayers. Monolayers were equally expanded over fcc-bridge-hcp domains of the reconstructed gold surface.

Neither ISA nor COR is chiral; however the COR/ISA network was found to be chiral on both substrates: HOPG and Au(111). The analysis revealed that the unit cell vectors of chiral domains were rotated by $+14 \pm 4°$ (clockwise) or $-14 \pm 4°$ (counterclockwise) with respect to the main lattice axis, ⟨110⟩, of gold. If we represent the COR/ISA heterocluster by a hexagon (blue feature in Figure 4B), we can easily define the smallest angle between one of the sides of the hexagon and a ⟨110⟩ symmetry axis of gold, which is $30 \pm 2°$. In other words, the sides of the hexagon run parallel to the ⟨211⟩ axis of the Au(111) substrate.

One- (DBA-OC10) and Three-Component (DBA-OC10/COR/ISA) Networks on Au(111). The substrate affects the adsorption strength of the different components. This in turn effects the concentrations and stoichiometric ratios of the components required in solution for successful self-assembly.

DBA-OC10 forms a porous network at the 1-octanoic acid/HOPG interface only at concentrations below 1.0×10^{-5} M (Figure S3A). At higher concentrations a combination of a high-density linear and the porous phase is formed. In comparison, on Au(111) even at the lowest concentrations probed (2.1×10^{-6} M) the high-density linear pattern is dominant (Figure S3B). The preference of the high density linear pattern on Au(111) for concentrations lower than those that produce a porous pattern on HOPG suggests stronger adsorption of DBA-OC10 molecules on Au(111) as opposed to HOPG.

It has been shown previously that a more complex three-component system (DBA-OC10/COR/ISA in 1-octanoic acid) on HOPG leads to a nanoporous network with the same chiral arrangement as a monocomponent DBA network (Figure S4).[36] For the three-component system 1-octanoic acid is used as a solvent because of poor solubility of ISA in TCB. Each chiral pore was occupied by a COR/ISA complex. In the STM image for a three-component system on Au(111) the central COR and six surrounding ISA molecules can be clearly identified as individual bright features within the DBA nanowells (Figure 5A; chiral nanowells are overlaid with blue hexagons). For the three-component system the optimum ratio of components in solution for self-assembly on Au(111) was 1.0:1.8:1100 for DBA-OC10, COR, and ISA, with a DBA-OC10 concentration of 1.1×10^{-6} M, while a 8.0×10^{-5} M concentration solution of

DBA-OC10 and saturated solutions of COR and ISA were optimized on HOPG.

Formation of the three-component networks was observed at much lower concentrations of the components on Au(111) as compared to HOPG, suggesting each component has a greater adsorption strength on Au(111). The stoichiometric composition of the solution also changes, with reduced fractions of COR and ISA relative to DBA-OC10 required on Au(111). The relative increase in adsorption strength is not the same for each component, with COR experiencing a greater relative increase as compared to DBA-OC10. Increasing the proportion of COR and ISA to a ratio of 1.0:5.4:3300 led to the formation of separated COR/ISA domains (Figure S5).

The three-component network (DBA-OC10/COR/ISA) in 1-octanoic acid on Au(111) shows a superlattice structure with the same morphology as seen for the two-component system on Au(111). The basis of this *superlattice* structure is also a chiral nanowell surrounded by six achiral nanowells (Figure 5A) with the following unit cell parameters: $a = b = 6.8 \pm 0.2$ nm, $\gamma = 66.0 \pm 2°$. However, in contrast to the two-component system well-ordered domains of three-component networks did not extend for areas larger than 50 × 50 nm (Figure S6). Increasing the number of components increases the complexity of the system and the self-assembly process, resulting in smaller domain sizes. A molecular model showing the details of the superlattice arrangement is given in Figure 5B.

Formation of the Superlattice. Deposition of premixed solutions of the relevant components allowed the formation of two- and three-component networks on Au(111) (Figures 3B and 5A, respectively). The networks on Au(111) are similar to those observed on HOPG, showing a porous framework of DBA with each pore containing either a COR in the case of the two-component network (Figure 3B) or a COR/ISA complex in the case of the three-component network (Figure 5A). In contrast to HOPG however, multicomponent networks on Au(111) display an ordered pattern of both chiral and achiral nanowells within individual nanoporous domains. The formation of this superlattice structure is exclusive to multicomponent systems on Au(111) and expanded equally over fcc-bridge-hcp domains of reconstructed Au(111). The formation and control of similar superlattice structures is an area of major interest in 2D supramolecular self-assembly.[43,44]

The driving force behind the formation of the superlattice structure for multicomponent systems on Au(111) can be understood in terms of energetic differences between different pore arrangements (chiral and achiral) and varying diffusion barriers of components on the different substrates.

It is the combination of a different substrate and the inclusion of COR or COR/ISA complexes that forms the superlattice. Molecular modeling simulations were performed according to a previously developed method[45] to address the differences in stability of

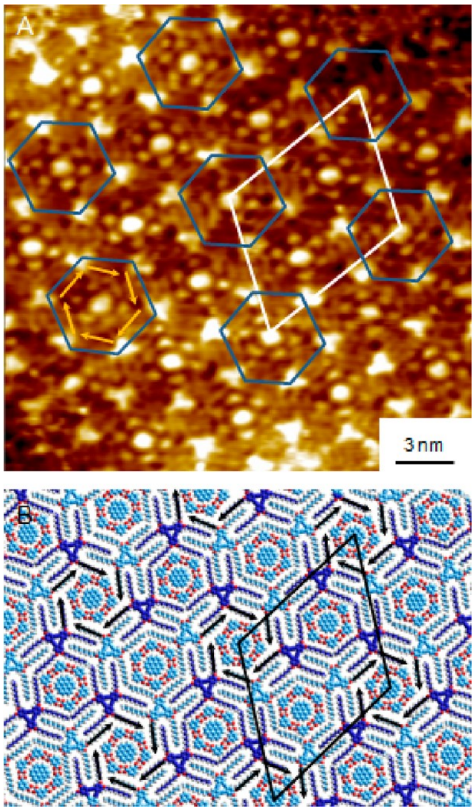

Figure 5. (A) STM image of three-component network (DBA-OC10/COR/ISA) in 1-octanoic acid on Au(111), $C_{(DBA\text{-}OC10)} = 1.1 \times 10^{-6}$ M, $C_{(COR)} = 2.0 \times 10^{-6}$ M, $C_{(ISA)} = 1.2 \times 10^{-3}$ M; conditions: $I_{set} = 248$ pA, $V_{set} = -465$ mV. $C_{(X)}$ reflects the concentration of component X in the supernatant solution prior to adsorption. Overlapping blue hexagons indicate chiral nanowells; yellow arrows along alkyl chains indicate the chirality of the nanowell. The white outline indicates the unit cell of the superlattice. (B) Molecular model showing the superlattice structure on Au(111); the black outline indicates the unit cell of the superlattice. Black arrows along alkyl chains indicate chirality of the nanowells (chiral nanowells).

chiral and achiral pores for multicomponent systems on HOPG and Au(111). The simulated systems consist of a monocomponent DBA-OC10 nanowell and multicomponent systems with a DBA-OC6 or DBA-OC10 nanowell with incorporated COR or COR/ISA complex, respectively. Figure 6 shows all models for molecular dynamic simulation on Au(111). Complete illustrations of these structures on HOPG and Au(111) are given in Figures S7, S8, and S9.

A summary of the results of the molecular modeling simulations is presented in Table 1, and details of the simulations are given in C.4, SI.

The parameter ΔE_{ads} is defined as the adsorption energy of the achiral arrangement minus the adsorption energy of the chiral arrangement. Positive values of ΔE_{ads} relate to chiral nanowells being more stable than achiral ones. For HOPG large positive values of ΔE_{ads} are observed (11.9 and 14.8 kcal mol^{-1} for the two- and three-component systems, respectively), while on Au(111) the values are significantly smaller (ΔE_{ads} = 3.4 and 2.3 kcal mol^{-1}). This disparity is also

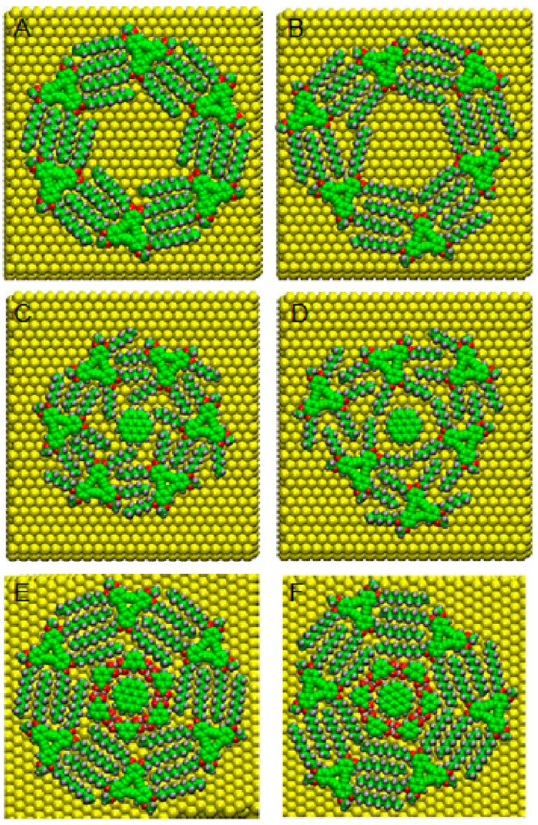

Figure 6. Molecular models showing the simulated structures on Au(111) for (A) chiral and (B) achiral nanowells for the monocomponent DBA-OC10 system; (C) chiral and (D) achiral nanowells for the two-component DBA-OC6/COR system; and (E) chiral and (F) achiral nanowells for the three-component DBA-OC10/COR/ISA system.

present in the monocomponent system (DBA-OC10) in the absence of the COR/ISA complex (on HOPG ΔE_{ads} = 6.4 kcal mol^{-1}, while on Au(111) ΔE_{ads} = 2.5 kcal mol^{-1}).

Larger values of ΔE_{ads} on HOPG compared to Au(111) are related to the registry between the zigzag alkoxy chain (−CH_2−CH_2−CH_2−) of the DBA molecule of the chiral nanowell and hexagonal skeletal carbon rings along the [010] vector of the HOPG lattice.[46,47,42] This match leads to certain orientations of alkyl chains with respect to the underlying HOPG being energetically favorable. The perfect hexagonal nature of chiral nanowells means that all of their alkyl chains can adopt the same orientation with respect to the HOPG. In contrast to this, the distorted hexagonal shape of an achiral nanowell means that alternating pairs of interdigitated alkyl chains around the nanowell have to adopt different orientations with respect to the HOPG (see simulation results Figure S9). This leads to a difference in stability between chiral and achiral nanowells on HOPG and large values of ΔE_{ads}. Au(111) does not show the same registry between alkyl chains and the substrate with a geometric mismatch between the spacing of CH_2 groups in alkyl chains (0.251 nm)[48] and the atomic periodicity of Au(111) (0.288 nm neglecting the herringbone reconstruction). This lack of a strong

TABLE 1. Calculated Adsorption Energies of Chiral and Achiral Nanowells for Monocomponent DBA-OC10, Two-Component DBA-OC6/COR, and Three-Component DBA-OC10/COR/ISA Systems, Formed on the Surfaces of HOPG and Au(111) As Determined by Molecular Mechanics Simulations[a]

substrate	pore type	E_{ads}, kcal/mol	ΔE_{ads}, kcal/mol
	Monocomponent System DBA-OC10		
au(111)	chiral	−198.5	2.5
	achiral	−196.0	
HOPG	chiral	−233.8	6.4
	achiral	−227.4	
	Two-Component System DBA-OC6/COR		
Au(111)	chiral	−93.9	3.4
	achiral	−90.5	
HOPG	chiral	−87.4	11.9
	achiral	−75.5	
	Three-Component System DBA-OC10/COR/ISA		
Au(111)	chiral	−336.2	2.3
	achiral	−333.8	
HOPG	chiral	−311.7	14.8
	achiral	−296.9	

[a] The energy values are per unit cell, with the unit cell for each simulation shown in Figures S7, S8, and S9.

registry between the adsorbed alkyl chains and the Au(111) results in smaller values of ΔE_{ads}. These differences in stability of the different pore arrangements explain why achiral pores are more likely to be observed on Au(111) than on HOPG. They do not however explain the formation of the superlattice.

To understand why the superlattice forms, we need to consider differences in diffusion barriers of the guest molecules/complexes (COR or COR/ISA) on the different substrates. Diffusion barriers (E_{dif}) for small aromatic molecules on Au(111) are significantly higher than on HOPG. On Au(111) E_{dif} was measured for benzene by tracking the motion of single molecules with STM as 3.39 kcal mol^{-1},[49] while on HOPG E_{dif} was measured by spin−echo spectroscopy to have a value of 0.39 kcal mol^{-1}.[50] Benzene, COR, and ISA are all small aromatic compounds and can be expected to follow a similar trend. These values for E_{dif} were obtained under UHV conditions, while the experiments reported here are carried out at the solid−liquid interface. The presence of solvent will play a key role in determining the diffusion barriers. Solvent molecules have to be displaced in order for DBA molecules to diffuse across the surface. Therefore the adsorption energy of the solvent molecule will directly influence the height of the diffusion barriers. It should be noted that because of the trend of larger adsorption energies for solvent molecules on metallic surfaces, this argument also suggests the presence of higher diffusion barriers on Au(111) as opposed to HOPG. The low diffusion barrier for guests on HOPG makes them less effective nucleation sites. Instead, the strong energetic preference for

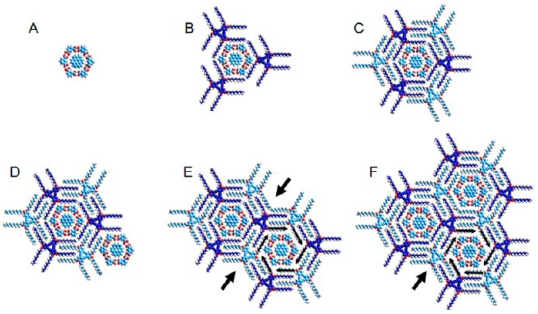

Figure 7. Molecular models showing step-by-step growth of the superlattice. (A) Initial nucleation around a COR/ISA cluster. (B) The alkyl chains of three DBA molecules surround the COR/ISA cluster. (C) The only way to complete a pore now is by the formation of an achiral pore. (D) A COR/ISA cluster is captured in one of the neighboring pores, which forms into either a chiral or achiral arrangement. (E) The model shows formation of a second chiral pore. (F) The model shows the formation of a third achiral pore on the arrow position. The large black arrows in (E) and (F) indicate positions where the structural arrangement of pores is predetermined by the combination of structures for the initial two pores (either achiral–achiral or achiral–chiral). Black arrows along alkyl chains in (E) and (F) indicate chirality of the pore.

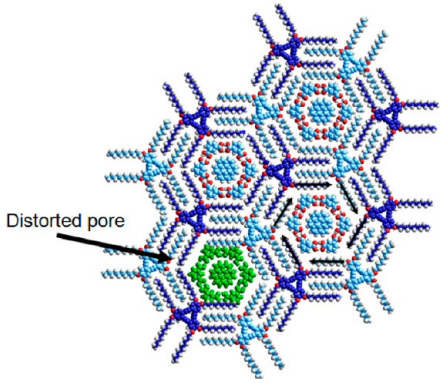

Figure 8. Model showing the hypothetical formation of a distorted pore.

chiral pores dominates the growth process, and domains consisting of only chiral pores are formed. The high diffusion barriers present on Au(111) however make the guests much more efficient nucleation sites.

If we consider the growth of multicomponent networks as a pore-by-pore process, the initial combination of pore structures (chiral or achiral) has direct implications for the overall network structure. Figure 7 shows a schematic of a step-by-step growth of the three-component network. A single COR/ISA cluster (Figure 7A) acts as a nucleation point; an identical process is expected for the two-component network with COR as the nucleation point. If we assume that in the initial stages of growth COR/ISA clusters act as nucleation points for the formation of an achiral pore (Figure 7A–C), then the superlattice arises from simple rules that govern the subsequent growth of the network.

Neighboring pores can now form into either chiral or achiral arrangements. The example in Figure 7D, E shows the formation of a chiral pore adjacent to the initial achiral pore. Importantly, this cluster of two adjacent achiral/chiral pores now imposes limitations on the sites marked by arrows in Figure 7E. At these sites the only way to complete a pore is by the formation of either an achiral pore (Figure 7F) or a distorted pore (Figure 8).

The formation of distorted pores will be unfavorable, as their interior dimensions are too small to capture a guest molecule or complex. If the second pore to form is an achiral pore (giving two achiral nanowells), then the sites marked by arrows in Figure 7E, by the same argument, are forced to form as chiral pores (Figure S10). From these simple rules we can see that if either the first or the second pore to form is achiral, then the growth of the ordered superlattice structure is observed. The overall morphology of the network is predetermined by the structural arrangement at the initial nucleation site.

CONCLUSIONS

We have demonstrated the formation of multicomponent networks at the liquid–solid interface between Au(111) and an organic solvent. These results are compared to previously reported work on an identical system formed on HOPG. Differences arise in the ratios and concentrations of components in the solution that are required for formation of the multicomponent networks. These differences are directly related to the strength of adsorption of the components on the different substrates. Formation of multicomponent networks on Au(111) results in a superlattice structure consisting of an ordered arrangement of chiral and achiral pores. This is in contrast to multicomponent systems on HOPG, where only chiral pores are observed. The formation of this superlattice is related to increased diffusion barriers on Au(111), which allow guest species to act as nucleation sites favoring the formation of achiral pores. The nucleation of an initial achiral pore in combination with some simple growth rules automatically produces the superlattice structure. The substrate has subtle effects on both the adsorption energy of molecules and their ability to act as nucleation sites. The study of such phenomena allows us to develop design criteria for even more complex self-assembled architectures on a wider variety of substrates.

MATERIALS AND METHODS

All experiments were performed at room temperature (20–24 °C) using a PicoSPM (Agilent) system operating in constant-current mode with the tip immersed in the supernatant liquid. STM tips were prepared by mechanical cutting of Pt/Ir wire (80%/20%, diameter 0.25 mm). Substrates consisted of either Au(111) films on mica (Georg Albert PVD Company) or HOPG (grade ZYB, Advanced Ceramics Inc., Cleveland, OH, USA).

Immediately prior to use Au(111) substrates were annealed in a butane flame and HOPG substrates were freshly cleaved. Reconstruction lines of Au(111) were not always present after sample annealing. For each measurement a 8 μL drop of the desired solution was applied directly to the prepared substrates and STM imaging commenced immediately. 1-Octanoic acid (Sigma, 99%) and 1,2,4-trichlorobenezene (TCB, Sigma-Aldrich, 99%) were used as solvents without further purification.

Conflict of Interest: The authors declare no competing financial interest.

Supporting Information Available: Details of synthesis for DBA derivative. Additional STM data. Molecular modeling details and results. This material is available free of charge *via* the Internet at http://pubs.acs.org.

Acknowledgment. This work is supported by the Fund of Scientific Research−Flanders (FWO), KU Leuven (GOA), the Belgian Federal Science Policy Office through IAP-6/27, Grant-in-Aid for Scientific Research from the Ministry of Education, Culture, Sports, Science, and Technology, Japan (21245012, 23111710), and the start-up funding of HIT, New Century Excellent Talents in University (NCET), from the Ministry of Education of P. R. China and the National Science Foundation of China (21173061).

REFERENCES AND NOTES

1. Surin, M.; Samori, P. Multicomponent Monolayer Architectures at the Solid-Liquid Interface: Towards Controlled Space-Confined Properties and Reactivity of Functional Building Blocks. *Small* **2007**, *3*, 190–194.
2. Griessl, S. J. H.; Lackinger, M.; Jamitzky, F.; Markert, T.; Hietschold, M.; Heckl, W. A. Incorporation and Manipulation of Coronene in an Organic Template Structure. *Langmuir* **2004**, *20*, 9403–9407.
3. Tahara, K.; Yamaga, H.; Ghijsens, E.; Inukai, K.; Adisoejoso, J.; Blunt, M. O.; De Feyter, S.; Tobe, Y. Control and Induction of Surface-Confined Homochiral Porous Molecular Networks. *Nat. Chem.* **2011**, *3*, 714–719.
4. Ecija, D.; Seufert, K.; Heim, D.; Auwarter, W.; Aurisicchio, C.; Fabbro, C.; Bonifazi, D.; Barth, J. V. Hierarchic Self-Assembly of Nanoporous Chiral Networks with Conformationally Flexible Porphyrins. *ACS Nano* **2010**, *4*, 4936–4942.
5. Matena, M.; Riehm, T.; Stohr, M.; Jung, T. A.; Gade, L. H. Transforming Surface Coordination Polymers into Covalent Surface Polymers: Linked Polycondensed Aromatics Through Oligomerization of N-Heterocyclic Carbene Intermediates. *Angew. Chem., Int. Ed.* **2008**, *47*, 2414–2417.
6. Lipton-Duffin, J. A.; Ivasenko, O.; Perepichka, D. F.; Rosei, F. Synthesis of Polyphenylene Molecular Wires by Surface-Confined Polymerization. *Small* **2009**, *5*, 592–597.
7. Gyarfas, B. J.; Wiggins, B.; Zosel, M.; Hipps, K. W. Supramolecular Structures of Coronene and Alkane Acids at the Au(111)-Solution Interface: A Scanning Tunneling Microscopy Study. *Langmuir* **2005**, *21*, 919–923.
8. MacLeod, J. M.; Ivasenko, O.; Fu, C. Y.; Taerum, T.; Rosei, F.; Perepichka, D. F. Supramolecular Ordering in Oligothiophene-Fullerene Monolayers. *J. Am. Chem. Soc.* **2009**, *131*, 16844–16850.
9. Kampschulte, L.; Lackinger, M.; Maier, A. K.; Kishore, R. S. K.; Griessl, S.; Schmittel, M.; Heckl, W. M. Solvent Induced Polymorphism in Supramolecular 1,3,5-Benzenetribenzoic Acid Monolayers. *J. Phys. Chem. B* **2006**, *110*, 10829–10836.
10. Mali, K. S.; Lava, K.; Binnemans, K.; Feyter, S. Hydrogen Bonding *versus* van der Waals Interactions: Competitive Influence of Noncovalent Interactions on 2D Self-Assembly at the Liquid-Solid Interface. *Chem.—Eur. J.* **2010**, *16*, 14447–14458.
11. Lackinger, M.; Heckl, W. M. Carboxylic Acids: Versatile Building Blocks and Mediators for Two-Dimensional Supramolecular Self-Assembly. *Langmuir* **2009**, *25*, 11307–11321.
12. Blunt, M. O.; Russell, J. C.; Champness, N. R.; Beton, P. H. Templating Molecular Adsorption Using a Covalent Organic Framework. *Chem. Commun.* **2010**, *46*, 7157–7159.
13. Shi, Z.; Liu, J.; Lin, T.; Xia, F.; Liu, P. N.; Lin, N. Thermodynamics and Selectivity of Two-Dimensional Metallosupramolecular Self-Assembly Resolved at Molecular Scale. *J. Am. Chem. Soc.* **2011**, *133*, 6150–6153.
14. Stepanow, S.; Lingenfelder, M.; Dmitriev, A.; Spillmann, H.; Delvigne, E.; Lin, N.; Deng, X. B.; Cai, C. Z.; Barth, J. V.; Kern, K. Steering Molecular Organization and Host-Guest Interactions Using Two-Dimensional Nanoporous Coordination Systems. *Nat. Mater.* **2004**, *3*, 229–233.
15. Stohr, M.; Wahl, M.; Galka, C. H.; Riehm, T.; Jung, T. A.; Gade, L. H. Controlling Molecular Assembly in Two Dimensions: The Concentration Dependence of Thermally Induced 2D Aggregation of Molecules on a Metal Surface. *Angew. Chem., Int. Ed.* **2005**, *44*, 7394–7398.
16. Pawlak, R.; Clair, S.; Oison, V.; Abel, M.; Ourdjini, O.; Zwaneveld, N. A. A.; Gigmes, D.; Bertin, D.; Nony, L.; Porte, L. Robust Supramolecular Network on Ag(111): Hydrogen-Bond Enhancement through Partial Alcohol Dehydrogenation. *ChemPhysChem* **2009**, *10*, 1032–1035.
17. Pawin, G.; Wong, K. L.; Kwon, K.-Y.; Bartels, L. A Homomolecular Porous Network at a Cu(111). *Surf. Sci.* **2006**, *313*, 961–962.
18. Lingenfelder, M. A.; Spillmann, H.; Dmitriev, A.; Stepanow, S.; Lin, N.; Barth, J. V.; Kern, K. Towards Surface-Supported Supramolecular Architectures: Tailored Coordination Assembly of 1,4-Benzenedicarboxylate and Fe on Cu(100). *Chem.—Eur. J.* **2004**, *10*, 1913–1919.
19. Zhang, X.; Chen, T.; Chen, Q.; Deng, G.-J.; Fan, Q.-H.; Wan, L.-J. One Solvent Induces a Series of Structural Transitions in Monodendron Molecular Self-Assembly from Lamellar to Quadrangular to Hexagonal. *Chem.—Eur. J.* **2009**, *15*, 9669–9673.
20. Arrigoni, C.; Schull, G.; Bleger, D.; Douillard, L.; Fiorini-Debuisschert, C.; Mathevet, F.; Kreher, D.; Attias, A.-J.; Charra, F. Structure and Epitaxial Registry on Graphite of a Series of Nanoporous Self-Assembled Molecular Monolayers. *J. Phys. Chem. Lett.* **2010**, *1*, 190–194.
21. Schull, G.; Douillard, L.; Fiorini-Debuisschert, C.; Charra, F.; Mathevet, F.; Kreher, D.; Attias, A.-J. Selectivity of Single-Molecule Dynamics in 2D Molecular Sieves. *Adv. Mater.* **2006**, *18*, 2954–2957.
22. Adisoejoso, J.; Tahara, K.; Okuhata., S.; Lei, S.; Tobe, Y.; De Feyter, S. Two-Dimensional Crystal Engineering: A Four-Component Architecture at a Liquid−Solid Interface. *Angew. Chem., Int. Ed.* **2009**, *48*, 7353–7357.
23. Ha, N. T. N.; Gopakumar, T. G.; Gutzler, R.; Lackinger, M.; Tang, H.; Hietschold, M. Influence of Solvophobic Effects on Self-Assembly of Trimesic Acid at the Liquid-Solid Interface. *J. Phys. Chem. C* **2010**, *114*, 3531–3536.
24. Furukawa, S.; Uji-i, H.; Tahara, K.; Ichikawa, T.; Sonoda, M.; De Schryver, F. C.; Tobe, Y.; De Feyter, S. Molecular Geometry Directed Kagome and Honeycomb Networks: Toward Two-Dimensional Crystal Engineering. *J. Am. Chem. Soc.* **2006**, *128*, 3502–3503.
25. Meier, C.; Roos, M.; Kuenzel, D.; Breitruck, A.; Hoster, H. E.; Landfester, K.; Gross, A.; Behm, R. J.; Ziener, U. Concentration and Coverage Dependent Adlayer Structures: From Two-Dimensional Networks to Rotation in a Bearing. *J. Phys. Chem. C* **2010**, *114*, 1268–1277.
26. Lei, S. B.; Tahara, K.; De Schryver, F. C.; Van der Auweraer, M.; Tobe, Y.; De Feyter, S. One Building Block, Two Different Supramolecular Surface-Confined Patterns: Concentration in Control at the Solid-Liquid Interface. *Angew. Chem., Int. Ed.* **2008**, *47*, 2964–2968.
27. Bellec, A.; Arrigoni, C.; Schull, G.; Douillard, L.; Fiorini-Debuisschert, C.; Mathevet, F.; Kreher, D.; Attias, A.-J.; Charra, F. Solution-Growth Kinetics and Thermodynamics of Nanoporous Self-Assembled Molecular Monolayers. *J. Chem. Phys.* **2011**, *134*, 124702.
28. Gutzler, R.; Sirtl, T.; Dienstmaier, J. F.; Mahata, K.; Heckl, W. M.; Schmittel, M.; Lackinger, M. Reversible Phase Transitions in Self-Assembled Monolayers at the Liquid-Solid Interface: Temperature-Controlled Opening and Closing of Nanopores. *J. Am. Chem. Soc.* **2010**, *132*, 5084–5090.

29. Katsonis, N.; Marchenko, A.; Fichou, D. Substrate-Induced Pairing in 2,3,6,7,10,11-Hexakis-Undecalkoxy-Triphenylene Self-Assembled Monolayers on Au(111). *J. Am. Chem. Soc.* **2003**, *125*, 13682–13683.
30. Kudernac, T.; Sandig, N.; Landaluce, T. F.; van Wees, B. J.; Rudolf, P.; Katsonis, N.; Zerbetto, F.; Feringa, B. L. Intermolecular Repulsion through Interfacial Attraction: Toward Engineering of Polymorphs. *J. Am. Chem. Soc.* **2009**, *131*, 15655–15659.
31. Xie, Z. X.; Xu, X.; Mao, B. W.; Tanaka, K. Self-Assembled Binary Monolayers of n-Alkanes on Reconstructed Au(111) and HOPG Surfaces. *Langmuir* **2002**, *18*, 3113–3116.
32. Bonini, M.; Zalewski, L.; Breiner, T.; Dotz, F.; Kastler, M.; Schadler, V.; Surin, M.; Lazzaroni, R.; Samori, P. Competitive Physisorption Among Alkyl-Substituted pi-Conjugated Oligomers at the Solid-Liquid Interface: Towards Prediction of Self-Assembly at Surfaces from a Multicomponent Solution. *Small* **2009**, *5*, 1521–1526.
33. Langner, A.; Tait, S. L.; Lin, N.; Rajadurai, C.; Ruben, M.; Kern, K. Self-Recognition and Self-Selection in Multicomponent Supramolecular Coordination Networks on Surfaces. *Proc. Natl. Acad. Sci. U. S. A.* **2007**, *104*, 17927–17930.
34. MacLeod, J. M.; Ivasenko, O.; Perepichka, D. F.; Rosei, F. Stabilization of Exotic Minority Phases in a Multicomponent Self-Assembled Molecular Network. *Nanotechnology* **2007**, *18*, 424031.
35. Xue, Y.; Zimmt, M. B. Patterned Monolayer Self-Assembly Programmed by Side Chain Shape: Four-Component Gratings. *J. Am. Chem. Soc.* **2012**, *134*, 4513–4516.
36. Lei, S.; Surin, M.; Tahara, K.; Adisoejoso, J.; Lazzaroni, R.; Tobe, Y.; De Feyter, S. Programmable Hierarchical Three-Component 2D Assembly at a Liquid-Solid Interface: Recognition, Selection, and Transformation. *NANO Lett.* **2008**, *8*, 2541–2546.
37. Tahara, K.; Furukawa, S.; Uji-i, H.; Uchino, T.; Ichikawa, T.; Zhang, J.; Mamdouh, W.; Sonoda, M.; De Schryver, F. C.; De Feyter, S.; *et al*. Two-Dimensional Porous Molecular Networks of Dehydrobenzo 12 Annulene Derivatives *via* Alkyl Chain Interdigitation. *J. Am. Chem. Soc.* **2006**, *128*, 16613–16625.
38. Lei, S.; Tahara, K.; Feng, X.; Furukawa, S.; De Schryver, F. C.; Muellen, K.; Tobe, Y.; De Feyter, S. Molecular Clusters in Two-Dimensional Surface-Confined Nanoporous Molecular Networks: Structure, Rigidity, and Dynamics. *J. Am. Chem. Soc.* **2008**, *130*, 7119–7129.
39. Zacharia, R.; Ulbricht, H.; Hertel, T. Interlayer Cohesive Energy of Graphite from Thermal Desorption of Polyaromatic Hydrocarbons. *Phys. Rev. B* **2004**, *69*, 155406.
40. Chakarova-Kack, S. D.; Schroder, E.; Lundqvist, B. I.; Langreth, D. C. Application of van der Waals Density Functional to an Extended System: Adsorption of Benzene and Naphthalene on Graphite. *Phys. Rev. Lett.* **2006**, *96*, 146107.
41. Rubes, M.; Kysilka, J.; Nachtigall, P.; Bludsky, O. DFT/CC Investigation of Physical Adsorption on a Graphite (0001) Surface. *Phys. Chem. Chem. Phys.* **2010**, *12*, 6438–6444.
42. Wetterer, S. M.; Lavrich, D. J.; Cummings, T.; Bernasek, S. L.; Scoles, G. Energetics and Kinetics of the Physisorption of Hydrocarbons on Au(111). *J. Phys. Chem. B* **1998**, *102*, 9266–9275.
43. Liu, J.; Chen, T.; Deng, X.; Wang, D.; Pei, J.; Wan, L.-J. Chiral Hierarchical Molecular Nanostructures on Two-Dimensional Surface by Controllable Trinary Self-Assembly. *J. Am. Chem. Soc.* **2011**, *133*, 21010–21015.
44. Xiao, W.; Feng, X.; Ruffieux, P.; Gröning, O.; Müllen, K.; Fasel, R. Self-Assembly of Chiral Molecular Honeycomb Networks on Au(111). *J. Am. Chem. Soc.* **2008**, *130*, 8910–8912.
45. Sandig, N.; Zerbetto, F. Molecules on Gold. *Chem. Commun.* **2010**, *46*, 667–676.
46. Groszek, A. J. Selective Adsorption at Graphite/Hydrocarbon Interfaces. *Proc. R. Soc. London A: Mat.* **1970**, *314*, 473–498.
47. Gellman, K. R. P. a. A. J. Effects of Conformational Isomerism on the Desorption Kinetics of *n*-Alkanes from Graphite. *J. Chem. Phys.* **2001**, *115*, 6737–6751.
48. Zhang, H. M.; Xie, Z. X.; Mao, B. W.; Xu, X. Self-Assembly of Normal Alkanes on the Au(111) Surfaces. *Chem.—Eur. J.* **2004**, *10*, 1415–1422.
49. Sykes, E. C. H.; Mantooth, B. A.; Han, P.; Donhauser, Z. J.; Weiss, P. S. Substrate-Mediated Intermolecular Interactions: A Quantitative Single Molecule Analysis. *J. Am. Chem. Soc.* **2005**, *127*, 7255–7260.
50. Hedgeland, H.; Fouquet, P.; Jardine, A. P.; Alexandrowicz, G.; Allison, W.; Ellis, J. Measurement of Single-Molecule Frictional Dissipation in a Prototypical Nanoscale System. *Nat. Phys.* **2009**, *5*, 561–564.